Case Studies in Thermal Engineering 61 (2024) 104947

Contents lists available at ScienceDirect

Case Studies in Thermal Engineering

journal homepage: www.elsevier.com/locate/csite

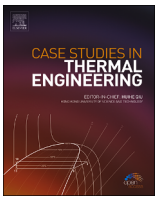

Manufacturing and performance of eco-efficient cementitious blocks for thermal cycling in thermal energy storage

Irene Ramón-Álvarez [a], Segundo Shagñay [a], Daniel Serrano [b], Antonio Caggiano [c], Manuel Torres-Carrasco [a,*], Sergio Sánchez-Delgado [b]

[a] University Carlos III of Madrid, Materials Sciences and Engineering Department-IAAB, Avda. Universidad 30, 28911, Leganés, Madrid, Spain
[b] University Carlos III of Madrid, Thermal and Fluids Engineering Department, Avda. Universidad 30, 28911, Leganés, Madrid, Spain
[c] Dipartimento DICCA, Università degli Studi di Genova, 16145, Genova, Italy

ARTICLE INFO

Keywords:
Alternative binders
Alkaline mortars
Hybrid mortars
Thermal energy storage
Heat recovery
Experimental analysis

ABSTRACT

Solar energy is a promising renewable option to provide energy demands in combination with conventional energy sources. However, to enhance the integration of renewable energies into the industrial section, it is necessary to employ thermal energy storage media. Among different thermal energy storage options, concrete has proven to be a very effective sensible thermal energy storage solution. However, its main raw material (i.e., the Portland cement), is the cause of huge CO_2 emissions to the environment. This study focuses on the design, manufacture, assembly and experimentation of thermal energy storage blocks made of alternative binders in substitution of Portland cement: i.e., hybrid materials and alkaline activated materials. The thermal energy storage blocks have been thermally cycled, with a charging temperature of 228 °C and a discharging temperature of 30 °C, in order to analyze the operational times and temperatures. The results obtained are very promising and comparable to those of the Portland cement system. Charging times have improved, with the alternative materials achieving temperature increases of up to 4%, while greater stabilization has been achieved during discharge, with the fluid reaching temperatures up to 6% higher than the reference system. These advancements support efficient, sustainable thermal energy storage technologies.

1. Introduction

A large part of the energy required by industry, more than 50%, is thermal energy. According to the International Renewable Energy Agency (IRENA), approximately 60% of heating demand is for industrial processes operating below 250 °C [1]. Nowadays, the main sources used to provide heat energy are fossil fuels [1,2]; however, due to global warming (associated with greenhouse gas emissions, where a 40% of the human-related CO_2 emissions come from burning fossil fuels), the limited sources of fossil fuels (oil supply is expected to end around 2050 due to high oil consumption) and the increases of the fuel prices [1,2], there is a growing interest in implementing renewable energies, such as solar thermal energy [1,3], to replace conventional sources or at least in reducing fossil fuel consumption by harnessing all the heat from the industrial process [4,5].

Industry mainly consumes heat energy for process/space heating, steam/hot water generation and product manufacturing [1]. When considering the heating process, a broad temperature range is compromised by thermal energy demand; nevertheless, the majority of thermal energy used is in the range of 30 °C–250 °C [3,6]. This range includes the temperatures defined as low and medium,

* Corresponding author.
E-mail address: matorres@ing.uc3m.es (M. Torres-Carrasco).

https://doi.org/10.1016/j.csite.2024.104947
Received 15 May 2024; Received in revised form 30 July 2024; Accepted 6 August 2024
Available online 12 August 2024

since low temperature is below 120 °C and medium temperature does not reach 400 °C. High temperature refers to processes that are over 400 °C [3,6].

Sterilisation, pasteurisation, polymerization, boiling, freezing and cooling, melting, painting, drying, cooking, hydrolysing, desalination, distillation and evaporation or washing and cleaning are common processes that use a low-medium temperature [1,7]. Solar energy is presented as an attractive renewable source to supply thermal energy to the described industrial processes [7]. For this purpose, there are many solar collectors available, but not all are suitable for process-heat applications. Flat-plate collectors (FPC) are the most commonly used technologies of solar systems, which in turn are the most traditional equipment. Standard FPC can easily achieve temperatures of up to 80 °C, but there are already FPC technologies available that can reach temperatures of up to 250 °C [8]. The introduction of highly-selective coatings is one of the causes of these temperature rises [9].

Considering the aforementioned, it is possible to combine traditional process heat generation systems with renewable solar energy systems. Because of the intermittent source of solar energy (due to night periods as well as cloudy days), the easiest way to successfully combine the systems is by introducing thermal energy storage (TES) devices [9]. TES systems are essential for efficient thermal management due to their ability to dispatch thermal energy even in periods of low or none irradiation, thus correcting the mismatch between the energy supply and demand [10,11]. In addition the TES systems are not only an indispensable element for solar thermal applications [11], but also they can be used as a key element for not wasting thermal energy generated in industrial processes from conventional sources [4,5]. This wasted thermal energy is also called Industrial Waste Heat (IWH), which is thermal energy that ends up in the environment and is underutilized [12,13]. This energy lost is due to the technical and economic difficulties in applying heat recovery methods and the mismatch between the energy released and its demand [12], and encompasses from low to high temperatures [13]. TES systems are a tool to recover the IWH, store it and use it when needed, reducing CO_2 emissions, leading to economic and energy savings and improving the overall efficiency of the industrial processes [2,12]. There are a variety of TES media that can be applied depending on temperature, power level and HTF [11]. One of the most common systems for TES, that has been used in many industrial processes, is storage using liquids. For the processes at low operational temperatures, liquid water is used as the main sensible heat storage [12,14], but when temperature exceeds 100 °C, non-pressurized liquid water cannot be used as a storage medium, and the water has to pressurized, with the issues that arise from this. There are other liquid storage media as oil or molten salts that can be used at higher temperature but count with degradation or high freezing points. To all of this, it is worth to mention the problems of managing these liquids once their lifetime has ended, and the great environmental impact in case of accident/leakage [14]. Thus, concrete is presented as a promising sensible heat storage medium that avoids these problems, provides good operational efficiency and has low investment and maintenance costs [10,15].

As a material, concrete counts with a high specific heat, which is an important key to keep the heat for longer time and allows a reduction in the storage volume, and presents good mechanical properties even after the exposure to thermal cycling. However, its thermal conductivity is quite low [16], which is directly related with the heat transfer velocity within the solid. To improve the performance of concrete as a TES system, multi-tubular cavities with embedded steel pipes (heat exchangers) are inserted into the concrete through which the HTF flows [17]. But caution should be exercised in the use of heat exchangers as these steel pipes account for at least the 50% of the total TES price [18]. For this reason, the block/heat exchanger design needs to be optimized (pipe diameter, number of pipes, arrangement of the pipes in the block, etc.) to achieve maximum transfer energy without neglecting the economic impact [19,20]. As it has been observed in previous studies, a triangular arrangement of pipes forming a 30° angle inside the concrete block optimized the heat transfer rate allowing the material to heat up faster [10]. In addition to the investment costs, the introduction of steel pipes leads to a reduction in strength, as the interface between the concrete block and the heat exchanger undergoes further degradation at high temperatures [21,22], therefore, due to the reasons presented above, it is preferable to not have pipes because of these functional and financial drawbacks.

Returning to the material qualities, concrete's impact on the environment is another drawback that frequently characterizes the material. Porland cement (PC), the main phase of concrete, is composed by clinker. Clinker production involves high energy consumption and gas emissions. Specifically, PC industry consumes a large sum of fossil fuel (which represents 12–15% of the total energy consumed in the industry) [23] and emits a large amount of polluting gases, in particular CO_2, which is estimated to account for 5–7% of global emissions [24,25]. To address environmental concerns, two alternatives were developed: the alkali-activated materials (AAM), so-called geopolymers, and the hybrid materials (HM).

AAM use aluminosilicate materials (that can be natural minerals or by-products of industrial processes) to fully substitute PC. To activate those aluminosilicate materials, it is necessary the use of an alkaline solution with high pH that limit the workability in the construction sector [26,27]. In contrast, the HM alternative is based on a mixture of PC, but in low content (20–30%), with aluminosilicate materials as the main precursor (70–80%). In this case, the aluminosilicate material is activated with soft alkaline salts (commonly used in a solid state) just in presence of water [28].

Considering the high percentage of thermal energy consumed at low-medium temperature (30 °C to 250 °C), the need to have TES devices (both to support solar renewable energies when the sun is not available as well as to recover the IWH) and the environmental drawbacks that PC offers in its manufacture (although it is proving to be an optimal means of storing thermal energy in the form of sensible heat), this study proposes the fabrication of TES prototypes composed of alternative materials to PC. AAM and HM systems were manufactured following the principles of the circular economy using blast furnace slag as their main precursor. The use of this by-product means a significant cost reduction together with environmental improvements, since it is waste from other industry that otherwise would end up in dumps, and its recycling leads to a decrease in the energy needed in the manufacturing process [23,29]. Replacing PC with low percentages of fly ash, slag, silica fume, and their combinations has been shown to decrease the thermal conductivity of concrete, a crucial property for TES operations [30]. However, some studies have found that these materials, when used as a complete replacement for PC, perform well at temperatures below 1000 °C [31,32]. Indeed, studies have demonstrated that AAM

withstand higher operating temperatures and thermal cycles than PC systems, exhibiting higher thermal storage capacity [10,33] and comparable thermal conductivity [34]. The reaction products formed in AAM can endure temperatures up to 800 °C with minimal structural degradation of the gel, thus achieving greater thermal stability than the C–S–H phase in traditional cement-based materials [35]. Additionally, cementitious materials developed from waste have shown fewer phase transitions and excellent thermal properties after undergoing several thermal cycles [31,34]. A TES prototype using AAM as the solid storage medium demonstrated that the heat storage capacity of the AAM-based system was 2–3.5 times higher than that of the patented Heatcrete® with a PC-based system [33]. These findings highlight the potential application of AAM for high-temperature TES in the future.

However, the environmental impact of these alternatives that completely replace PC, AAM, must be considered, as they require strong alkaline solutions, which also pose significant environmental challenges. Previous studies [15,36] have shown that these solutions have a substantial impact on both the carbon and water footprints. Therefore, exploring other systems, such as HM, is crucial as their functionality as TES is less documented in the literature. Further research is needed to optimize TES, given that the study of these alternatives is attracting interest due to the limited number of scientific articles available, with most research focusing primarily on fire resistance [34,37].

Therefore, in order to check the feasibility and stability of the alternative materials as TES, thermal charging/discharging cycles between 30 °C and 228 °C were performed, using air as HTF. The effects on these mortars at these temperature ranges highly demanded by the industry are unknown, as the materials have not been investigated computationally or experimentally before. The flow rate of the HTF was monitored by a volume flow meter before passing it through a prototype TES that was fabricated for this study. In order to measure the temperature evolution within the TES block during the heating/cooling processes, thermocouples were placed in the block of all systems. In addition to acquiring the mass loss evolution along the block, the mass of the block before and after 8 thermal cycles was measured to study how temperature influences this parameter. Mass loss in these temperature ranges is directly related to water evaporation [37,38]. This evaporation of the water trapped in the pores influences the thermal conductivity of the material since, as only air remains in the pores, the heat transfer given inside the block decreases due to the low conductivity of the dry air [39]. These acquired data provide information about the operational times of materials such as TES. In this way, it can be seen how fast the materials heat up during the charging process and how long it will be possible to supply energy to the HTF without the source being available during the discharging. All these results have been collected for a reference system made of PC and for its two alternatives, AAM and HM systems, in order to be compared.

2. Experimental procedure

2.1. Mortar selection

Three types of mortars were performed: a reference sample, made of PC and referred as PC; an AAM, made of an industrial by-product (a blast furnace slag) referred as SLAG, and a HM, composed of a mixture of the two aforementioned binder materials and referred as HSLAG. The selection of these mortars was decided in consequence of previous studies, where the alternative materials were shown to be comparable or even better than PC according to different properties.

2.1.1. Mechanical properties

Previous studies using high temperatures with more critical thermal cycles (20 series from 200 °C to 400 °C or exposure to temperatures up to 500 °C) for the application of these mortars as TES in concentrated solar power (CSP) thermal plants [10,15] have experimentally demonstrated that SLAG mortar presents the best mechanical performance. As this system was manufactured using sodium silicate, the C-A-S-H gel (generated from the slag) has a high cohesion and compaction due to the silicon added in the solution [26,40]. Thanks to this behavior, the compressive strength value of the SLAG remains almost constant after thermal exposure, decreasing by only 5% (which means a +80% of improvement compared to PC). As for HSLAG, it was found that after the thermal treatment, a reaction took place in the material that generated new binders [41] that conferred a higher compressive strength, increasing its value by +6% compared to the reference PC system.

2.1.2. Thermal properties

In addition to good mechanical performance, in terms of thermal properties, both alternative materials have been shown to be comparable to PC [15,39,42]. Regarding the thermal conductivity and the specific heat capacity, they are greatly affected (like the mechanical strengths) by porosity and cracks [16], affected into the material by heat treatments. Pores and cracks can hinder the propagation of phonons at atomistic scale, resulting in the interruption of heat transfer within the material [43,44]. Other factors impacting thermal properties under temperature exposure include chemical reactions, particle size, material bonding, moisture content, crystallinity, and aging [45]. Taking into account these effects in thermal properties, it was studied how the thermal conductivity as well as the specific heat of the materials was affected by temperature [10], finding that alternative binder systems offer promising results. In particular, SLAG improved its thermal conductivity compared to PC by 16%. Both SLAG and HSLAG demonstrated substantial improvements in specific heat, which is directly related to energy storage, by 46% and 21%, respectively. By studying both thermal properties, porosity and density (both at room temperature [39] and after cycling [10]), it has been possible to simulate heat transfer problems using *ANSYS Fluent* or FEM simulation. These simulations predict the experimental behavior of the materials. Thus, due to previous experience, in this research study we have chosen the reference system as well as the AAM and HM systems to compare and obtain a real behavior of these materials as TES.

In the present work, the temperature study range, due to the experimental equipment and the objective of this research, is now between 30 °C and 228 °C in order to experimentally study their viability as TES of process heat. Previous simulations conducted at dif-

ferent temperature ranges indicated that these alternative materials performed better than the PC system [10,39], particularly at higher temperatures (up to 400 °C), where PC suffered significant degradation. However, the behavior of these materials at lower temperatures remains unknown due to a lack of both computational and experimental studies. The study of these materials has not been done either computationally or experimentally for lower temperature ranges, so it is not known how the systems will be affected. In addition, it should be noted that none of the simulations already published have taken into account the transformation processes that the material undergoes during the heating/cooling cycles, such as shrinkage/expansion of the aggregates/binder [46–48], evaporation of water, mass loss of the aggregates [49], decomposition of the gels and components [47,50–52], among others. All these factors affecting the heat transfer in the material and its use as a TES, have been determinant to carry out an experimental test to determine the stability of the systems, the heating/cooling times, and the stored energy in each system.

2.1.3. Life cycle assessment

Although the environmental impact of the materials does not influence their performance as TES, it is important to note that the previous life cycle assessments (LCA) that have been carried out on these alternative materials resulted in significant improvements in both carbon and water footprints compared to the reference PC mortar. These assessments demonstrated over a 100% reduction in CO_2 emissions and up to a 40% reduction in water consumption [15,36].

2.2. Materials

For the manufacture of these three mortars (PC, SLAG and HSLAG), the two binders used were Portland cement I 42.5R, supplied by the company "*Cementos Portland Valderrivas*", and the blast furnace slag from ENSIDESA (Avilés, Spain). Their chemical composition are shown in Table 1: both contain high contents of CaO, SiO_2 and Al_2O_3.

2.3. Samples preparation

For the preparation of the mortars, the UNE EN 196-1 [53] standard was followed. The following mixtures were prepared.

- PC mortar: Portland cement CEM I 42.5R and aggregate (sand) (wt. ratio 1:3 respectively) hydrate just in presence of water.
- SLAG mortar: blast furnace slag and aggregate (sand) (wt. 1:3 ratio) were used. A commercial solution of sodium silicate (waterglass) diluted with water and NaOH to achieve a SiO_2/Na_2O ratio equal to 0.8 was used to activate the mixture.
- HSLAG mortar: 77.5 wt% of slag and 17.5 wt% of CEM I 42.5R. In addition, the HM systems contain a soft alkaline activator, specifically, 5 wt% of Na_2SO_4 was added to accelerate the hydration process that it is produced with water [54]. This percentage addition of Na_2SO_4 was determined to be optimal based on previous studies [34,39]. These systems were also prepared with a precursor/aggregate (sand) ratio of 1:3 wt%.

To provide the same workability in all systems, the liquid/solid (L/S) ratios were varied following the UNE EN 1015-6 standard [55]. Table 2 shows the exact quantities of each component to manufacture the different systems. The mortar was poured into a rectangular mould (140 × 160 × 40 mm^3) after the mixing in an automatic laboratory mixer (five molds were used for each storage system). To improve the mortar distribution in the rectangular mould, the Proeti automatic compactor was used according to the UNE 196-3 standard [56]. Then, the specimens were cured during 28 days in a humid climate container (99% relative humidity), at room temperature (22 °C) before they were tested.

2.4. Prototype fabrication

The TES block, called system, is composed by five slabs of mortar. Geometry and dimensions (mm) of those slabs are shown in Fig. 1. As ducts through which the HTF flows, it was decided to make prototypes with cylindrical passages avoiding the use of steel pipes, since, as mentioned above, they have significant economic and functional disadvantages. According to a prior study [10], a 12 mm diameter of the cylindrical passages, or hollows, is optimal for an HTF to flow through to transfer or absorb the heat. It was demonstrated that a triangular pipe distribution increases the system efficiency, being the heating of blocks faster than a square distribution. For this reason, the cylindrical passages in the slabs are arranged in a triangle way.

Table 1
Chemical composition of the raw materials (%wt) by XRF.

%wt	CaO	SiO_2	Al_2O_3	MgO	Fe_2O_3	SO_3	Na_2O	K_2O	*LoI
PC CEM I 42.5R	61.94	21.28	6.45	< 0.003	2.53	5.87	< 0.012	1.01	2.35
Blast furnace SLAG	35.73	36.15	11.75	12.750	0.38	1.75	< 0.010	0.27	2.10

*LoI: loss on ignition.

Table 2
Mortar preparation.

Nomenclature	Raw material (g)	Addition	L/S	Water (g)	Activator solution (g)	Aggregate (g)
PC	450-PC	–	0.50	225-H_2O	–	1350-S
SLAG	450-SLAG	–	0.55	–	247.5-Na_2SiO_3 Solution	1350-S
HSLAG	348.75-SLAG 78.75-PC 22.5-Na_2SO_4	5% Na_2SO_4	0.46	207-H_2O	–	1350-S

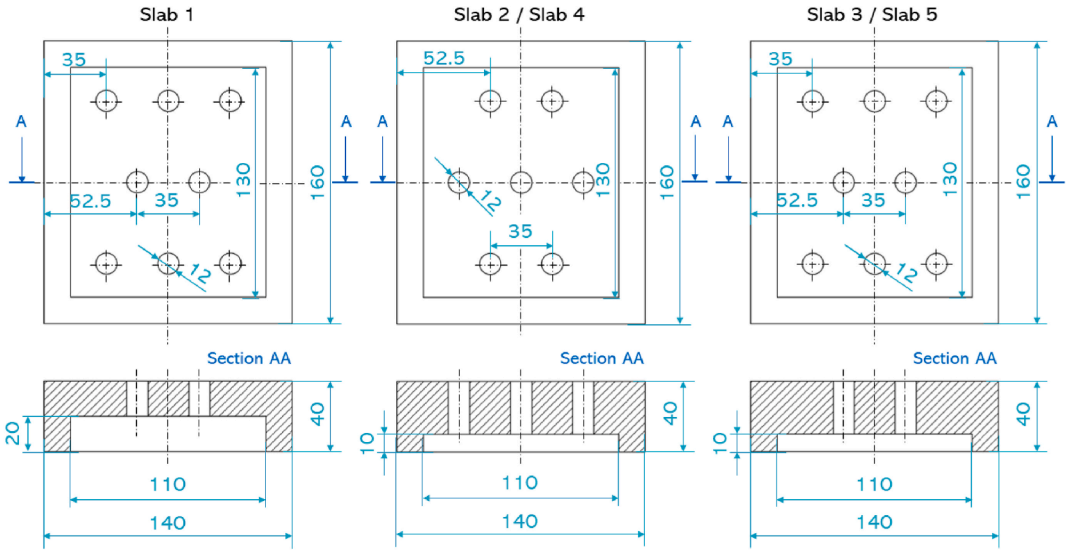

Fig. 1. Plans of the slabs.

In order to manufacture the mortar slabs, the elements described in Fig. 2 (a) are used. Slab 1, unlike the others, contains a gap of 20 mm in height. To create this hole, instead of a 10 mm steel plate, two steel plates were overlapped together inside the mould (elements described in the lower part of Fig. 2 (a)). The 20 mm high hole is used to insert stainless steel wool to distribute the incoming air into the block homogeneously, avoiding a preferred air path. After pouring the mortar in the final assembly (Fig. 2 (b)), a thermocouple is inserted into each slab 10 mm from the surface to collect temperature data during the charging and discharging processes. To properly demould the mortars, leaving the passages free, the cylinders were rotated during the setting process to prevent the adhesion of the cementitious material. After 24 h, the slab was extracted from the mould and was introduced in the humid climate for curing. The resulting slabs can be seen in Fig. 2 (c).

The distribution of holes is different in slabs 1, 3 and 5 compared to slabs 2 and 4. This is due to the fact that when the slabs are overlapped, the HTF (air in this case) does not just travel through a pipe with a linear inlet and outlet, increasing the contact area, the air turbulence and therefore, the heat transfer. The sequence of the slabs to form the TES system can be seen in Fig. 3.

To form the TES block, slabs were joined (following the order shown in Fig. 3) using a silicone sealant that resists high temperatures and stays flexible.

By this block assembly, the study of the thermal equilibrium between two bodies in contact is made possible. Fig. 4 illustrates how the block's temperature and the air flow's temperature will change as the charging cycle begins. In the charging process represented in Fig. 4, it can be seen how both elements (system and air) reach thermal equilibrium after an infinite time. In short, two bodies in equilibrium with a third are in equilibrium with each other (zeroth law of thermodynamics established by Ralph H. Fowler [57]). In this case study, the thermal equilibrium is reached when the two bodies equalize their initially different temperatures, due to the heat

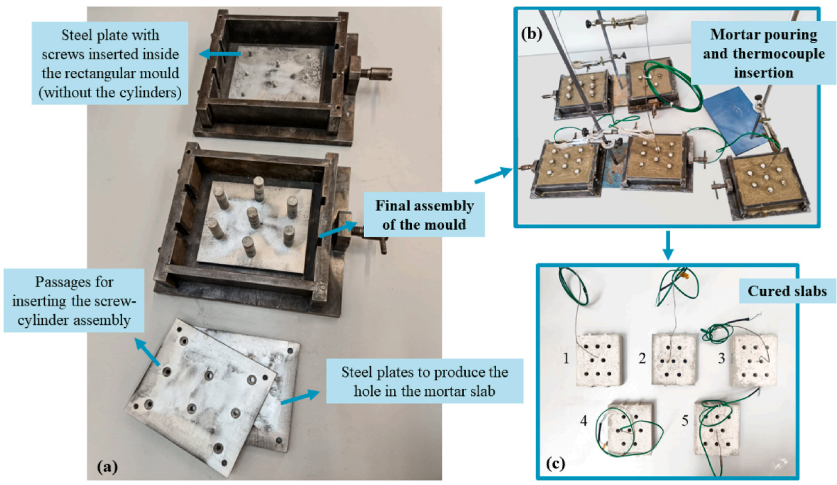

Fig. 2. (a) Assembly of the mould (b) Production of the slabs (c) Cured slabs.

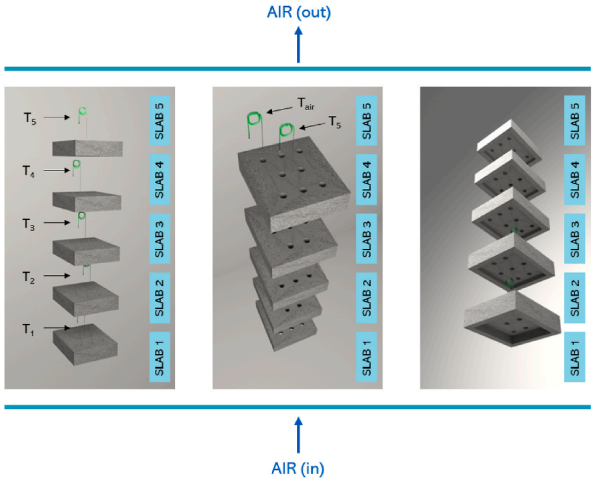

Fig. 3. Order of the slabs for the assembly of the TES blocks. The air flows from slab 1 to slab 5.

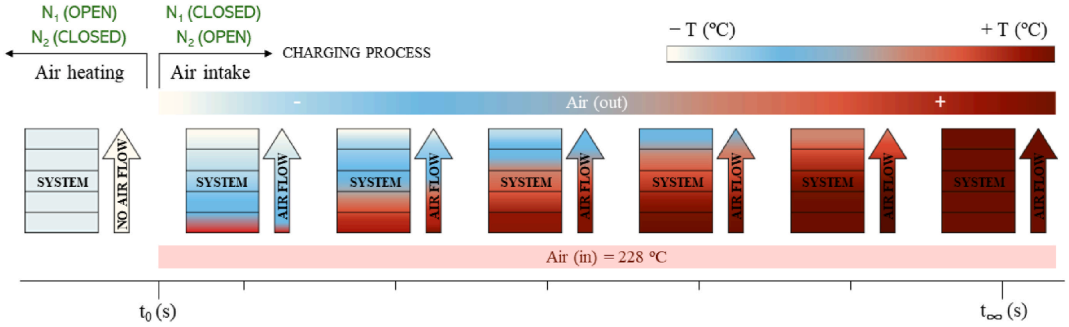

Fig. 4. Evolution of system and air flow temperatures during the charging process up to infinite time.

transfer from one body to the other. The air inlet temperature is fixed at 228 °C during the whole process. Since the incoming air is at 228 °C and the TES system is initially at room temperature (30 °C), the air gives up its energy to the system to heat it up. As air enters from the bottom, slab 1 is the first slab to absorb the heat. As a result, the air flow temperature will drop after crossing slab 1. However, after passing slab 1, the air will still have a higher temperature than slab 2, so the second slab will also heat up (although not as fast in the beginning as slab 1). The subsequent layers exhibit the same behavior. As the lower slabs reach higher temperatures, the air at the bottom will no longer give up as much heat as it did at the beginning of the test (there is a decrease in thermal inertia). Thus, after passing through the initial slabs, the air will hold a higher temperature which will heat the subsequent slabs, i.e. the air flow remains warmer at greater inlet distances. Finally, as can be seen in Fig. 4, for an infinite time, all the thermocouples (both those placed in the system (T_1 to T_5) and the thermocouple controlling the temperature of the air flow at the outlet (T_{out})) will end up measuring the same temperature (thermal equilibrium). This same behavior would be repeated in a discharging cycle, but in that process, as the air enters cold (30 °C) and the system is hot (228 °C), it is the TES system that would release its heat to the air, heating it. In this case, as the lower slabs come into contact with the cold air first, they will cool down faster than the upper slabs. This is because the air will have increased its temperature by the time it reaches the top of the TES block as it is absorbing the heat provided by the system during its travel. Thermal equilibrium would be reached in the discharge process when both elements (TES system and air flow) have a temperature of 30 °C.

In the study case, the test does not last an infinite time due to the limitations of the experiment (i.e., the air heater does not have a PID temperature controller). In this way, both the charging and discharging cycles, run for 3.5 h (enough time to stabilize the first slab temperature). This means that a complete test lasts 7 h (25,200 s). Fig. 5 represents how the system and air flow change their temperature during the test (charging and discharging processes). In this case, due to the time, thermal equilibrium could not be completed, but it can be observed how as the slabs heat up, the hot air is able to travel further. The same behavior occurs for the cooling stage; once the first slabs have cooled down (they are in contact with the HTF first), the air does not absorb the heat at the beginning of the system and is able to stay for a longer distance at a lower temperature to cool down the upper block. Shorter system charging times combined with a longer system discharge period that allows the system to retain heat and transfer it to the HTF are the most ideal conditions for the process [42].

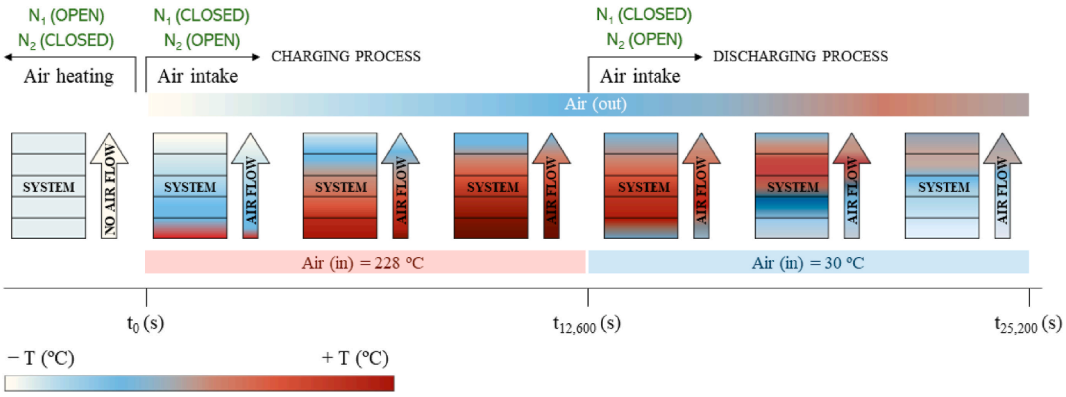

Fig. 5. Evolution of system and air flow temperatures during charging and discharging of the real experiment.

2.5. Equipment and procedure

The schematic overlapping of slabs is shown in Fig. 6, which also shows the experimental set-up where the control volume that is taken as a reference for the study is also specified. In addition to the TES block, this control volume has an aluminum plate, stainless steel wool that has been placed into the first slabs's 20 mm gap as previously indicated, two needle valves that control the direction of

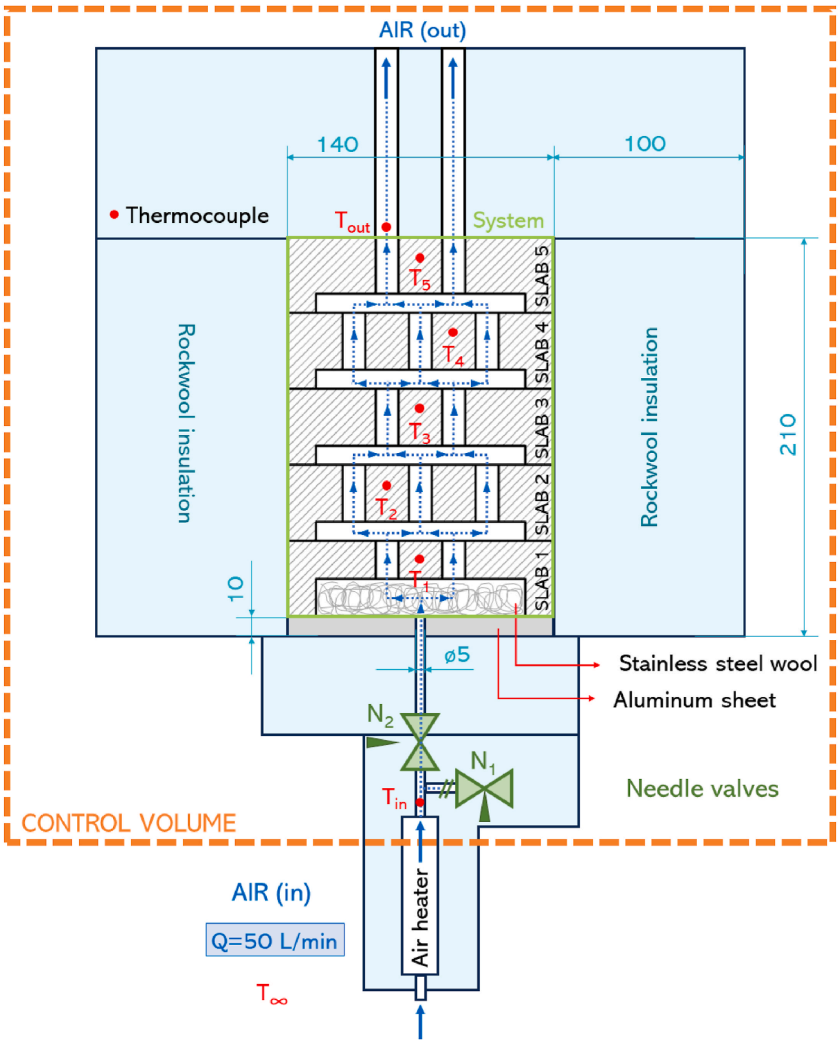

Fig. 6. Cross-section of the prototype: assembly of the five slabs with their respective control thermocouples. The block is thermally insulated with rockwool.

air flow and their connections. In this way, as it can be seen in Fig. 6, the air flow does not only affect the cementitious block, but also the other components described. That means that the thermal energy supplied will not only heat the cementitious system, but it is possible to make a comparison between materials as all three have the same assembly.

The air heating system and data collection (Fig. 7) were assembled in addition to the control volume. The Watlow Fluent device is used to heat the air. This heater, for operational requirement, must operate with a minimum air flow of 50 L/min, in order to reach the maximum air temperature. The flow rate was therefore set at 50 L/min, measured with a volume flowmeter connected to the air line. With the heater well insulated, the maximum air flow temperature that could be reached was 228 °C. Therefore, this temperature was defined as the inlet air temperature (T_{in}) in the charging cycles for all the experiments.

Finally, the block is placed on the aluminum plate on top of the structure. This aluminum plate has a passage for connecting the heater (see Fig. 6). The link between the mortar slabs and the block is joined to the aluminum sheet using a specific high temperature silicone sealant. This is done for two reasons: i) to promote the airtightness of the system by generating a better contact (air can only travel through the passages of the block) and ii) because, in addition, it has been seen that a horizontal structure made of graphite or aluminum provides greater heat transfer [49].

Once the equipment is assembled, thermal cycles were performed. First, for the charging process, the central valve (N_2) shown in Fig. 6 is closed while the side valve (N_1) is open. This is done at the beginning of the process until the heater reaches the desired temperature and can heat the air to 228 °C. Once the charging temperature is reached (temperature is checked with the control thermocouple (T_{in})), the position of both valves is changed to direct the flow of 50 L/min into the system. Thus, the side valve is closed (N_1) and the central valve is opened (N_2), as shown in Fig. 6, to allow hot air into the block, at this moment the charging cycle starts. At the end of the charging cycle, the discharging process starts by setting the temperature of the air heater to 30 °C. The air-cooling time is negligible compared to the total test time, as with the T_{in} thermocouple, it was found that the air flow reached the cooling temperature in about 30 s.

The charging/discharging procedure is repeated for 8 cycles, which is when it is observed that the temperature of slab 1 of each material remains stable (as the temperature has not changed from the previous cycle 7). Furthermore, conducting 8 thermal cycles of exposure provides insights into the degradation of the material. It should be noted that mechanical and thermal properties are predominantly affected after the first cycle. These thermal cycling studies are particularly interesting because there is little literature addressing the effects of thermal cycling on cementitious materials intended for use in TES applications [34,58].

Charging/discharging temperatures make it possible to study the range where thermal energy is most consumed (between 30 °C and 250 °C [3]). Charging and discharging cycles of 3.5 h (12,600 s) are performed (i.e. the complete study duration is 7 h). This test time is set because it is enough for the first slab to reach a steady state as its temperature does not present remarkable variation with time i.e. the variation of the slab temperature over time converges to zero value (see Fig. 8). For the last cycle, the time when slab 1, of each system, reaches the greatest temperature variation is between seconds 40 and 50 of the test. At the end of the test, the derivative maintains its value around 0, which indicates that the slab cannot reach a higher temperature.

During the 7 h (25,200 s) of the test, data is taken every 5 s using LabVIEW 2019 software. Data collection is obtained thanks to the Ni 9210 acquisition cards, whose offset error is ±20 μV maximum, where the 6 thermocouples, each with a tolerance of ±1.5 °C, are connected (5 belonging to each mortar slab - T_1, T_2, T_3, T_4 and T_5 - and 1 measuring the temperature of the air coming out through one of the cylindrical passages (T_{out})). The position of the thermocouples is shown in Fig. 6 represented by the red dots.

In addition to the measurement of the temperature variation, the whole block was weighed to note the mass before exposure to temperature. This value, together with the weight of the block after the thermal treatment, will give the mass loss of each system.

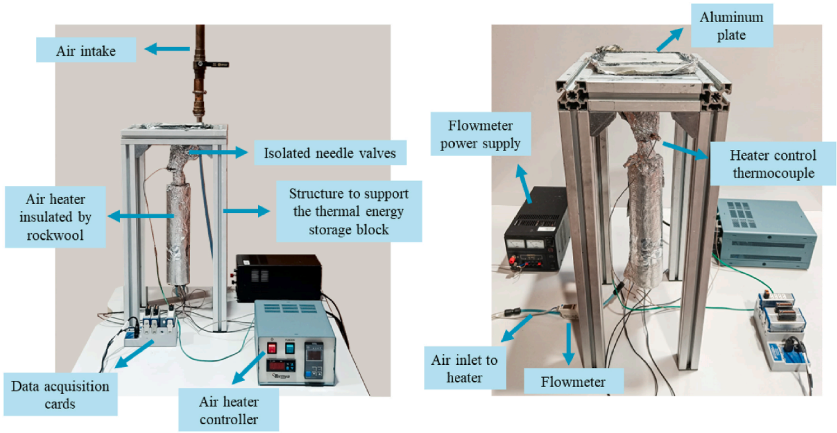

Fig. 7. Air heating and data collection system.

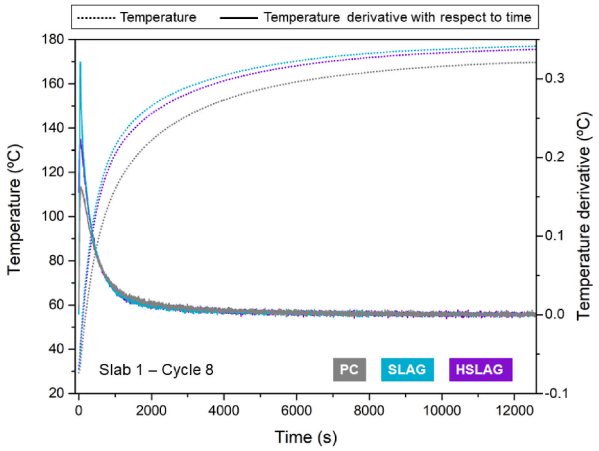

Fig. 8. Temperature and its derivative as a function of test time for slab 1 of each system in the last cycle performed (cycle number 8).

3. Results

3.1. Stability of systems against heating/cooling cycles

In addition to setting how long the test should last (Fig. 8), the number of cycles required for slab 1 of each system to stabilize was determined.

This number of cycles was the same for all the systems: i.e., 8 cycles. Fig. 9 shows the temperature evolution of the slab 1 of the three materials. All the mortars follow the same trend, as the cycles pass, they manage to reach a higher temperature after 3.5 h of charging until cycle 8 is performed, where the charging and discharging curve is almost the same as in cycle 7. This phenomenon occurs because in the first cycles the thermal energy is not only used to heat the material but also to evaporate the water trapped in the pores or chemically bound in the cementitious materials. Due to evaporation of the water, there is a mass loss that can be seen in Fig. 10. This mass loss is related to previous studies where PC is the system that loses the most mass in these temperature ranges, followed by SLAG and finally HSLAG. Comparing the percentage of mass loss of the alternative systems with the PC, the alternative systems lose around 15% less mass.

Consequently, the steepest increase between cycle 1 and 8 is reached by the PC system in both the charging and discharging process. Specifically, the PC curve of cycle 8 with respect to the first cycle suffers an increase of more than 10% for the final charge temperature and 13% for the final discharge temperature, while in the case of the SLAG it is more of 5% in the case of heating and suffers a decrease of almost 1% in the discharge process (Table 4). Regarding the HSLAG system, there are two increases for both the final charge and discharge temperature of more than 5% and 2%, respectively (Table 4). This can be seen graphically in Fig. 9 (where only the stabilization of the first slab after the thermal cycles is taken into account) and Fig. 11 (where the 5 slabs are compared as well as the air outlet temperature for cycle 1 and 8). It should be noted that the change in temperatures achieved between cycle 1 and cycle 8 after heating is a direct and primary consequence of the stabilization of the systems after water evaporation. However, it should be noted that in the three mortars, as seen in Fig. 11, the data collection in cycle 8 started with higher slab temperatures. The higher initial temperature is due to conducting the tests in a minimally warmer environment. However, the room temperature varied by at most 2 ˚C, neglecting its ultimate effects on the maximum temperature reached. Also, quantitatively, Table 3 shows the final charging (at 12,600 s) and discharging (at 25,200 s) temperature values, and Table 4 calculates the percentage increase/decrease of cycle 8 with respect to cycle 1 for each mortar.

PC uses more thermal energy in the first cycles, compared to SLAG or HSLAG, in evaporating the trapped water (as it has a greater amount of water than the other systems due to its greater porosity [10,15,39], as has been verified in Fig. 10 with the mass loss) than in heating up, for this reason the final curve is further away from the first cycles (see Figs. 9 and 11). The steeper curve is also noticeable in the cooling process for PC as the material can spend more time at a higher temperature giving up its heat to the air (as it has heated up more). On the other hand, this behavior does not occur in the alternative materials since the discharge curve remains almost stable by having a minimum increase or even a lower temperature in the last cycle compared to the first as mentioned in the percentages previously provided. This is due to the lower porosity of the alternative systems. As the alternative systems have fewer pores compared to PC, these mortars do not retain as much water. The water has a higher thermal conductivity than the air in the pores once the water has evaporated (see also [39,59,60]), so after the water has been removed, the alternative systems are able to conduct heat faster, giving up more energy to the HTF as they do not have as much porosity as PC. In addition to the voids generated by the elimination of water in the pores, the defects generated by exposure to temperature must be taken into account. Thermal stress leads to a deformation in the material between the aggregates and the binder, which produces the formation and propagation of cracks from the pores [46]. In this case, due to the thermal cycles, the materials are going to be affected by the expansion/contraction phenomena; where the aggregate expands during the heating, while the binder shrinks, leading to the generation of cracks [48]. On this point, the reference sample is more disadvantaged because the C–S–H gel is more incompatible with the aggregates than the C-A-S-H gel, as its thermal expansion coefficient is further away from that of the C-A-S-H gel with sand [61].

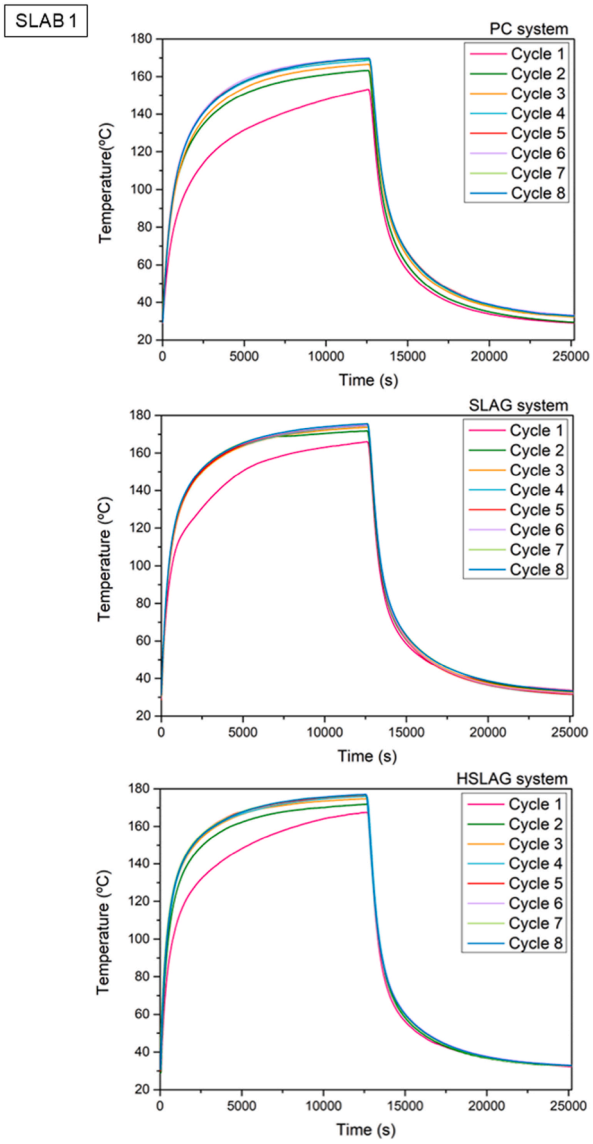

Fig. 9. Slab 1 evolution during the 8 cycles.

It is known that the thermal conductivity is mainly linked to the porosity/cracks found in the materials, however, there are also other factors that affect this thermal property such as the crystallinity of the raw materials. Thus, in previous studies, it was seen that the Portland cement raw material has a higher crystallinity than the blast furnace slag, so that the propagation of phonons is interrupted by the grain boundaries, decreasing heat transfer [39]. However, although the temperature difference in the discharge curve between cycle 1 and cycle 8 is minimal in the alternative materials and does not increase as in the case of PC, most of the temperatures measured by the thermocouples in the alternative materials are higher than in the case of PC (Table 3). The improvement of the alternative systems with respect to the PC for both cycle 1 and cycle 8 can be seen in Table 5.

Precisely, it is seen in Table 5 that the percentage increase in the final temperatures is greater in cycle 1 than in cycle 8 when comparing the alternative systems with the PC reference block. For example, for the slab 1 in the charging process, both alternative systems offer about 5% more increase in cycle 1 compared to cycle 8. As explained above, this is because the PC initially uses the thermal energy to evaporate the water instead of heating up like the alternative systems. When slab 1 of the systems stabilizes in cycle 8, we can observe that both alternative systems offer a higher temperature (Table 3) in slab 1 both at the end of charging and discharging processes. Specifically, in the case of the heating process, an improvement of more than 3% is obtained in the case of the SLAG and more than 4% in the case of the HSLAG for the slab number 1. Regarding discharge, although it may seem that the alternative systems would transfer their energy more quickly to the HTF (as they offer shorter warm-up times during charging), the reality is that they take longer to cool down, as they have stored more energy predictably. Thus, the final discharge temperature at slab 1 is more than 1% for SLAG and 0.22% for HSLAG when compared to the PC reference system.

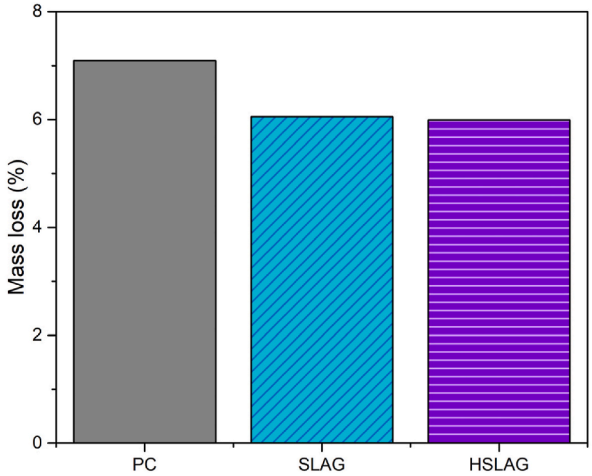

Fig. 10. Mass loss percentage after the 8 thermal cycles.

This means that during heating, the alternative materials heat up faster than the reference PC mortar and, during cooling, they can store thermal energy for a longer time by maintaining a high temperature while heating the HTF. Both phenomena can be seen graphically in Fig. 12.

It can be appreciated in Table 5 that, looking at the outlet air temperature, it is observed that the HTF acquires a higher temperature when passing through the alternative systems (at the end of heating, it gets about 5% warmer in the case of SLAG and almost 2% warmer for HSLAG compared to PC and, at the end of cooling, the air gets a temperature compared to PC of more than 6% in the case of SLAG and almost 4% for HSLAG). Faster operational warm-up times as well as higher discharge stability indicate greater efficiency of alternative materials such as TES.

This behavior can also be seen considering the temperature changes of all the slabs, as well as the temperature of the air at the outlet, with respect to the first slab (Table 6). At the end of the charging process, at 12,600 s, it is observed how the alternative systems present a greater temperature difference with respect to their first slab. This is because when the air has passed through the first plate, it has given up more heat in the alternative systems than in the PC. In other words, the alternative systems absorbed more thermal energy (heat) after the HTF passed through the first slab in order to reach thermal equilibrium. Thus, when the air reaches the successive slabs, it is cooler (as seen in Fig. 5) than in the case of the PC. Even though the HTF is cooler, the alternative systems still capture the heat given off by the air more quickly and in greater quantity, so that, as previously seen in the tables and figures, the PC is the system that reaches a lower temperature compared to the other two systems. As for the discharge, as can be seen in Table 6, the values of the alternative systems are also higher compared to those of the PC. This indicates that the slabs of the alternative systems cool down more slowly. Both the AAM and the HM can transfer their heat to the cold air and heat it for a longer time, causing it to reach a higher temperature at the outlet of the system at the end of the discharge process. These results suggest both a higher heat transfer in the alternative systems and a greater heat preservation (less material is required to store the same amount of energy), as demonstrated in previous studies using computational modelling and simulation [39,42].

In short, the results indicate that the alternatives are very comparable to the PC and even offer shorter charging times as well as greater stability during discharge by holding heat longer and increase the time of release it to the air due to their higher stored energy. This charging process behavior increases the system's efficiency by reducing operating times and heating the system to higher temperatures, thus achieving a higher sensible heat storage [62,63]. In addition, the fact that the alternative (greener) materials keep their heat longer in cooling indicates that they have stored more thermal energy. Achieving higher storage means that fewer blocks are needed to store a certain amount of energy, thus saving costs, resources and space [10].

4. Conclusions

After the design, manufacturing, assembly, and testing of the cementitious blocks in a temperature range of 30–228 °C after 8 thermal cycles, it can be stated that alternative (greener) materials are very comparable to Portland cement reference system in terms of thermal energy storage. Additionally, they can even offer shorter charging times (thereby improving the system's efficiency), as they heat up more quickly. For example, the first slab of the alternative systems shows an approximate 4% increase in temperature after the last charging cycle compared to the Portland cement reference system. In addition, alkali-activated and hybrid materials are capable of heating the heat transfer fluid to a higher temperature and for a longer time, when compared to Portland cement cementitious material. Consequently, considering the air flow temperature at the outlet after the discharge process in the final cycle, there is a temperature increase of 3.65% for the hybrid material and 6.42% for the alkali-activated material. This enhanced stability indicates greater thermal energy storage by alternative systems, which translates into cost, resource and space savings. The operational performance is strongly influenced by porosity, which affects both mechanical and thermal properties. The reference Portland cement system compared to the alternative systems leads to a higher mass loss (around 15%) after exposure to temperature. In the temperature ranges that have been investigated in this study, their mass loss is attributed only to water evaporation, which is higher in the Port-

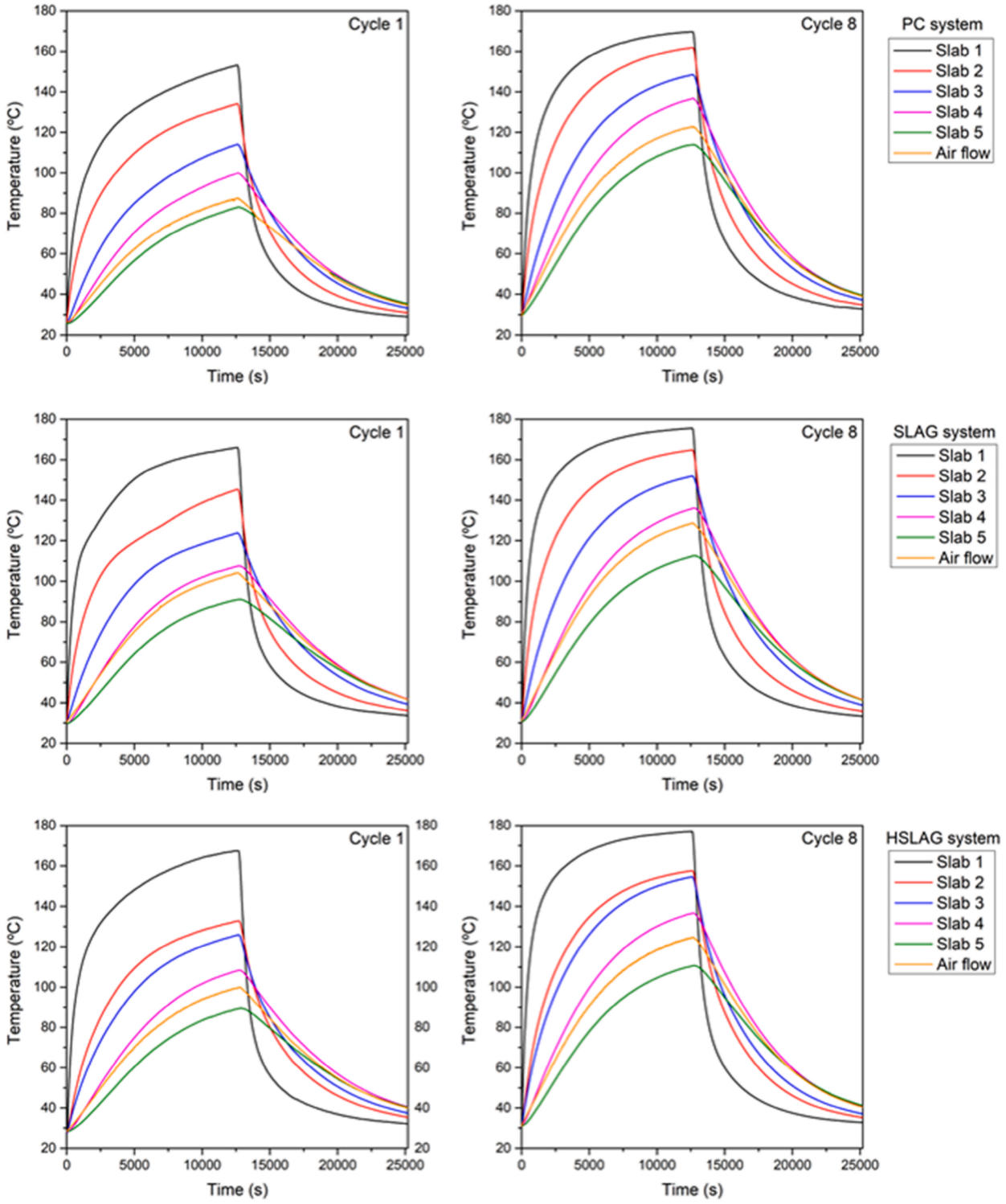

Fig. 11. Comparison between the heating/cooling curves of cycle 1 and cycle 8 of the three systems.

land cement block as it has more porosity where more water is trapped. Therefore, as we have seen, the Portland cement system uses thermal energy in the first cycles to carry out an evaporation process, instead of heating up, while the alternative systems do not use so much heat to evaporate the water but rather to heat up. The results obtained reveal that alternative systems are very promising for use as thermal energy storage. On the other hand, Portland cement system, while proving to be a good thermal energy storage solid

Table 3
Final temperatures after charging (at 12,600 s) and discharging (at 25,200 s) for each of the systems in cycle 1 (first one) and cycle 8 (last one).

	PC			
	Cycle 1		Cycle 8	
	T (^{0}C) (12,600 s)	T (^{0}C) (25,200 s)	T (^{0}C) (12,600 s)	T (^{0}C) (25,200 s)
SLAB 1 (T_1)	153.22	29.01	169.71	32.81
SLAB 2 (T_2)	134.21	30.88	161.87	34.73
SLAB 3 (T_3)	114.09	33.17	148.46	37.23
SLAB 4 (T_4)	99.84	35.15	136.72	39.37
SLAB 5 (T_5)	82.88	35.24	113.85	39.42
Air Flow (Tout)	87.35	34.64	122.43	38.99
	SLAG			
	Cycle 1		**Cycle 8**	
	T (^{0}C) (12,600 s)	T (^{0}C) (25,200 s)	T (^{0}C) (12,600 s)	T (^{0}C) (25,200 s)
SLAB 1 (T_1)	166.05	33.62	175.56	33.31
SLAB 2 (T_2)	145.36	36.02	164.77	35.69
SLAB 3 (T_3)	123.75	39.30	151.91	38.83
SLAB 4 (T_4)	107.42	41.83	135.87	41.56
SLAB 5 (T_5)	90.92	41.62	112.38	41.33
Air Flow (Tout)	104.12	41.63	128.67	41.49
	HSLAG			
	Cycle 1		**Cycle 8**	
	T (^{0}C) (12,600 s)	T (^{0}C) (25,200 s)	T (^{0}C) (12,600 s)	T (^{0}C) (25,200 s)
SLAB 1 (T_1)	167.51	32.19	177.02	32.88
SLAB 2 (T_2)	132.73	35.40	157.58	35.30
SLAB 3 (T_3)	125.83	37.44	154.57	37.09
SLAB 4 (T_4)	108.18	40.56	136.58	40.65
SLAB 5 (T_5)	89.20	40.33	110.56	41.19
Air Flow (Tout)	99.48	40.00	124.71	40.41

Table 4
Percentage change in charge and discharge temperatures of cycle 8 compared to cycle 1.

	PC		SLAG		HSLAG	
	Cycle 8 compared to Cycle 1 (%)		Cycle 8 compared to Cycle 1 (%)		Cycle 8 compared to Cycle 1 (%)	
	(12,600 s)	(25,200 s)	(12,600 s)	(25,200 s)	(12,600 s)	(25,200 s)
SLAB 1 (T_1)	+10.77	+13.09	+5.72	−0.93	+5.68	+2.12
SLAB 2 (T_2)	+20.61	+12.49	+13.36	−0.93	+18.71	−0.29
SLAB 3 (T_3)	+30.13	+12.22	+22.75	−1.20	+22.83	−0.94
SLAB 4 (T_4)	+36.94	+12.00	+26.48	−0.63	+26.26	+0.22
SLAB 5 (T_5)	+37.37	+11.87	+23.60	−0.70	+23.94	+2.13
Air Flow (Tout)	+40.16	+12.56	+23.58	−0.33	+25.36	+1.04

Table 5
Percentage changes in the final charge and discharge temperatures of the alternative materials compared to PC.

	SLAG				HSLAG			
	Cycle 1 compared to PC (%)		Cycle 8 compared to PC (%)		Cycle 1 compared to PC (%)		Cycle 8 compared to PC (%)	
	(12,600 s)	(25,200 s)	(12,600 s)	(25,200 s)	(12,600 s)	(25,200 s)	(12,600 s)	(25,200 s)
SLAB 1 (T_1)	+8.38	+15.90	+3.44	+1.53	+9.33	+10.98	+4.31	+0.22
SLAB 2 (T_2)	+8.30	+16.66	+1.79	+2.74	−1.10	+14.65	−2.65	+1.63
SLAB 3 (T_3)	+8.47	+18.47	+2.32	+4.31	+10.30	+12.87	+4.11	−0.37
SLAB 4 (T_4)	+7.59	+18.99	−0.63	+5.57	+8.35	+15.40	−0.10	+3.26
SLAB 5 (T_5)	+9.71	+18.10	−1.29	+4.84	+7.64	+14.45	−2.89	+4.48
Air Flow (Tout)	+19.19	+20.18	+5.09	+6.42	+13.88	+15.47	+1.86	+3.65

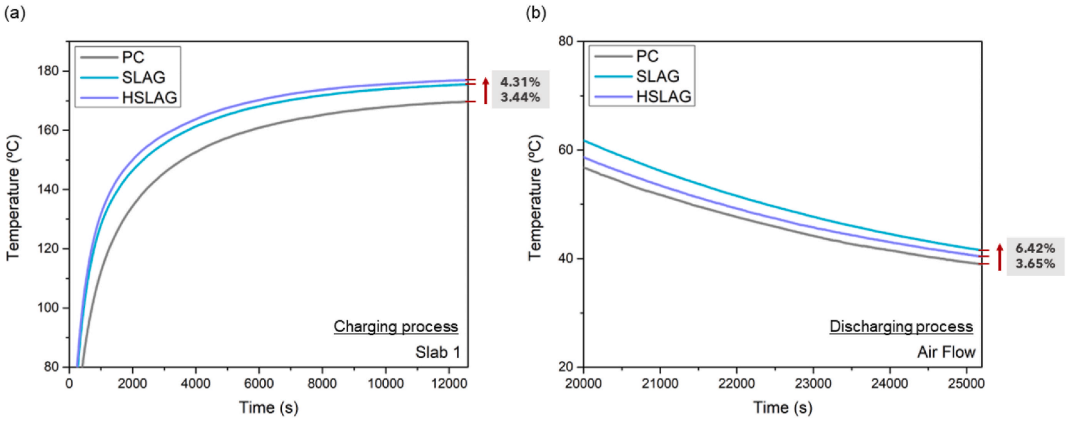

Fig. 12. Temperature evolution (a) at slab 1 during charging (b) of the air flow during discharging.

Table 6
Temperature change percentages of the slabs (2, 3, 4, 5) and the air outlet with respect to the first plate.

	PC		SLAG		HSLAG	
	Temperature change with respect to slab 1 in cycle 8 (%)		Temperature change with respect to slab 1 in cycle 8 (%)		Temperature change with respect to slab 1 in cycle 8 (%)	
	(12,600 s)	(25,200 s)	(12,600 s)	(25,200 s)	(12,600 s)	(25,200 s)
SLAB 1 (T_1)	–	–	–	–	–	–
SLAB 2 (T_2)	−4.62	+5.88	−6.14	+7.14	−10.99	+7.37
SLAB 3 (T_3)	−12.52	+13.48	−13.47	+16.59	−12.69	+12.82
SLAB 4 (T_4)	−19.44	+20.01	−22.61	+24.79	−22.84	+23.66
SLAB 5 (T_5)	−32.92	+20.17	−35.99	+24.09	−37.55	+25.28
Air Flow (Tout)	−27.86	+18.85	−26.71	+24.58	−29.55	+22.93

medium, brings with it serious environmental impacts. Therefore, there is a need to make way for new materials that, in addition to offering operational improvements in terms of energy efficiency, allow decarbonisation using industrial by-products.

CRediT authorship contribution statement

Irene Ramón-Álvarez: Writing – review & editing, Writing – original draft, Visualization, Supervision, Software, Resources, Methodology, Investigation, Conceptualization. **Segundo Shagñay:** Writing – original draft, Software, Methodology, Investigation. **Daniel Serrano:** Writing – original draft, Supervision, Software, Methodology, Investigation. **Antonio Caggiano:** Writing – review & editing, Writing – original draft, Visualization, Validation, Supervision, Methodology, Investigation. **Manuel Torres-Carrasco:** Writing – review & editing, Writing – original draft, Visualization, Validation, Supervision, Methodology, Investigation, Funding acquisition, Formal analysis. **Sergio Sánchez-Delgado:** Writing – review & editing, Writing – original draft, Visualization, Validation, Supervision, Software, Resources, Methodology, Investigation, Funding acquisition, Conceptualization.

Declaration of competing interest

The authors declare the following financial interests/personal relationships which may be considered as potential competing interests:Manuel Torres Carrasco reports financial support was provided by University Carlos III of Madrid. Manuel Torres Carrasco reports a relationship with University Carlos III of Madrid that includes: board membership and employment.

Acknowledgment

This study was funded by MCIN/AEI/10.13039/501100011033 and Europe Union NextGenerationEU/PRTR under the National Project TED2021-130633B–I00 and under the National Project PID2021-125810OB-C22. Funding for APC: Universidad Carlos III de Madrid (Agreement CRUE-Madroño 2024).

Data availability

No data was used for the research described in the article.

References

[1] N. Tasmin, S.H. Farjana, M.R. Hossain, S. Golder, M.A.P. Mahmud, Integration of solar process heat in industries: a review, Cleanroom Technol. (2022), https://doi.org/10.3390/cleantechnol4010008.

[2] G. Sadeghi, Energy storage on demand: thermal energy storage development, materials, design, and integration challenges, Energy Storage Mater. (2022), https://doi.org/10.1016/j.ensm.2022.01.017.

[3] Y. Gebreyohannes, M. Bayray, J. Lauwaert, A review on solar thermal utilization for industrial heating and cooling processes: global and Ethiopian perspective, momona ethiop, J. Sci. (2021), https://doi.org/10.4314/mejs.v12i2.6.

[4] A.I. Fernández, C. Barreneche, L. Miró, S. Brückner, L.F. Cabeza, Waste heat recovery using thermal energy storage, in: Adv. Therm. Energy Storage Syst. Methods Appl., 2020, https://doi.org/10.1016/B978-0-12-819885-8.00022-X.

[5] H. Slimani, Y. Filali Baba, H. Ait Ousaleh, A. Elharrak, F. El Hamdani, H. Bouzekri, A. Al Mers, A. Faik, Horizontal thermal energy storage system for Moroccan steel and iron industry waste heat recovery: numerical and economic study, J. Clean. Prod. (2023), https://doi.org/10.1016/j.jclepro.2023.136176.

[6] C.A. Schoeneberger, C.A. McMillan, P. Kurup, S. Akar, R. Margolis, E. Masanet, Solar for industrial process heat: a review of technologies, analysis approaches, and potential applications in the United States, Energy (2020), https://doi.org/10.1016/j.energy.2020.118083.

[7] A. Fernández-García, E. Rojas, M. Pérez, R. Silva, Q. Hernández-Escobedo, F. Manzano-Agugliaro, A parabolic-trough collector for cleaner industrial process heat, J. Clean. Prod. (2015), https://doi.org/10.1016/j.jclepro.2014.11.018.

[8] IEA-ETSAP, IRENA, Solar Heat for Industrial Processes -Technology Brief, 2015, p. 37. www.irena.org/Publications.

[9] S. Kalogirou, The potential of solar industrial process heat applications, Appl. Energy (2003), https://doi.org/10.1016/S0306-2619(02)00176-9.

[10] I. Ramón-Álvarez, S. Sánchez-Delgado, I. Peralta, A. Caggiano, M. Torres-Carrasco, Experimental and computational optimization of eco-friendly mortar blocks for high temperature thermal energy storage of concentrated solar power plants, J. Energy Storage (2023), https://doi.org/10.1016/j.est.2023.108076.

[11] R. Tamme, D. Laing, H. Müller-Steinhagen, W.-D. Steinmann, High temperature heat storage for industrial process heat and power generation, in: EUROSOLAR Conf, 2006.

[12] L. Miró, J. Gasia, L.F. Cabeza, Thermal energy storage (TES) for industrial waste heat (IWH) recovery: a review, Appl. Energy (2016), https://doi.org/10.1016/j.apenergy.2016.06.147.

[13] H. Jouhara, N. Khordehgah, S. Almahmoud, B. Delpech, A. Chauhan, S.A. Tassou, Waste heat recovery technologies and applications, Therm. Sci. Eng. Prog. (2018), https://doi.org/10.1016/j.tsep.2018.04.017.

[14] D. Laing, D. Lehmann, C. Bahl, E.Z. Ag, Concrete storage for solar thermal power plants and industrial process heat, Renew. Energy (2008).

[15] I. Ramón-Álvarez, E. Batuecas, S. Sánchez-Delgado, M. Torres-Carrasco, Mechanical performance after high-temperature exposure and Life Cycle Assessment (LCA) according to unit of stored energy of alternative mortars to Portland cement, Construct. Build. Mater. 365 (2023), https://doi.org/10.1016/j.conbuildmat.2022.130082.

[16] A. Gil, M. Medrano, I. Martorell, A. Lázaro, P. Dolado, B. Zalba, L.F. Cabeza, State of the art on high temperature thermal energy storage for power generation. Part 1-Concepts, materials and modellization, Renew. Sustain. Energy Rev. (2010), https://doi.org/10.1016/j.rser.2009.07.035.

[17] R. Kumar, A.K. Pathak, M. Kumar, A.K. Patil, Experimental study of multi tubular sensible heat storage system fitted with wire coil inserts, Renew. Energy (2021), https://doi.org/10.1016/j.renene.2020.10.058.

[18] U. Herrmann, D.W. Kearney, Survey of thermal energy storage for parabolic trough power plants, J. Sol. Energy Eng. Trans. ASME. (2002), https://doi.org/10.1115/1.1467601.

[19] C.R.C. Rao, H. Niyas, P. Muthukumar, Performance tests on lab–scale sensible heat storage prototypes, Appl. Therm. Eng. (2018), https://doi.org/10.1016/j.applthermaleng.2017.10.085.

[20] K. Bataineh, A. Gharaibeh, Optimal design for sensible thermal energy storage tank using natural solid materials for a parabolic trough power plant, Sol. Energy (2018), https://doi.org/10.1016/j.solener.2018.06.108.

[21] B. Zhang, H. Zhu, J. Chen, O. Yang, Evaluation of bond performance of corroded steel bars in concrete after high temperature exposure, Eng. Struct. (2019), https://doi.org/10.1016/j.engstruct.2019.109479.

[22] G. Ruano, F. Isla, B. Luccioni, R. Zerbino, G. Giaccio, Steel fibers pull-out after exposure to high temperatures and its contribution to the residual mechanical behavior of high strength concrete, Construct. Build. Mater. (2018), https://doi.org/10.1016/j.conbuildmat.2017.12.129.

[23] N. Shehata, E.T. Sayed, M.A. Abdelkareem, Recent progress in environmentally friendly geopolymers: a review, Sci. Total Environ. (2021), https://doi.org/10.1016/j.scitotenv.2020.143166.

[24] E. Benhelal, G. Zahedi, E. Shamsaei, A. Bahadori, Global strategies and potentials to curb CO2 emissions in cement industry, J. Clean. Prod. 51 (2013) 142–161, https://doi.org/10.1016/j.jclepro.2012.10.049.

[25] R. Feiz, J. Ammenberg, M. Eklund, A. Helgstrand, R. Marshall, Improving the CO2 performance of cement, part I: utilizing life-cycle assessment and key performance indicators to assess development within the cement industry, J. Clean. Prod. 98 (2015) 272–281, https://doi.org/10.1016/J.JCLEPRO.2014.01.083.

[26] F. Puertas, M. Torres-Carrasco, Use of glass waste as an activator in the preparation of alkali-activated slag. Mechanical strength and paste characterisation, Cem. Concr. Res. 57 (2014) 95–104, https://doi.org/10.1016/j.cemconres.2013.12.005.

[27] M. Torres-Carrasco, J.G. Palomo, F. Puertas, Sodium silicate solutions from dissolution of glass wastes: statistical analysis, Mater. Construcción 64 (2014), https://doi.org/10.3989/mc.201405213.

[28] I. Garcia-Lodeiro, N. Boudissa, A. Fernandez-Jimenez, A. Palomo, Use of clays in alkaline hybrid cement preparation. The role of bentonites, Mater. Lett. 233 (2018) 134–137, https://doi.org/10.1016/j.matlet.2018.08.098.

[29] I. Amer, M. Kohail, M.S. El-Feky, A. Rashad, M.A. Khalaf, Characterization of alkali-activated hybrid slag/cement concrete, Ain Shams Eng. J. (2021), https://doi.org/10.1016/j.asej.2020.08.003.

[30] R. Demirboğa, Thermal conductivity and compressive strength of concrete incorporation with mineral admixtures, Build. Environ. (2007), https://doi.org/10.1016/j.buildenv.2006.06.010.

[31] P. Keane, R. Jacob, N. Trout, S. Clarke, F. Bruno, Thermal stability of a waste-based alkali-activated material for thermal energy storage, Chem. Thermodyn. Therm. Anal. (2021), https://doi.org/10.1016/j.ctta.2021.100014.

[32] N.P. Tran, T.N. Nguyen, J.R. Black, T.D. Ngo, High-temperature stability of ambient-cured one-part alkali-activated materials incorporating graphene nanoplatelets for thermal energy storage, Dev. Built Environ. 18 (2024) 100447, https://doi.org/10.1016/j.dibe.2024.100447.

[33] M. Rahjoo, G. Goracci, J.J. Gaitero, P. Martauz, E. Rojas, J.S. Dolado, Thermal energy storage (TES) prototype based on geopolymer concrete for high-temperature applications, Materials (2022), https://doi.org/10.3390/ma15207086.

[34] I. Ramón-Álvarez, S. Sánchez-Delgado, M. Torres-Carrasco, Viability of hybrid and alkali-activated slag materials for thermal energy storage: analysis of the evolution of mechanical and thermal properties, J. Build. Eng. 95 (2024), https://doi.org/10.1016/j.jobe.2024.110073.

[35] Q. Song, M.Z. Guo, T.C. Ling, A review of elevated-temperature properties of alternative binders: supplementary cementitious materials and alkali-activated materials, Construct. Build. Mater. (2022), https://doi.org/10.1016/j.conbuildmat.2022.127894.

[36] E. Batuecas, I. Ramón-Álvarez, S. Sánchez-Delgado, M. Torres-Carrasco, Carbon footprint and water use of alkali-activated and hybrid cement mortars, J. Clean. Prod. (2021), https://doi.org/10.1016/j.jclepro.2021.128653.

[37] D. Suescum-Morales, J.D. Ríos, A.M. De La Concha, H. Cifuentes, J.R. Jiménez, J.M. Fernández, Effect of moderate temperatures on compressive strength of ultra-high-performance concrete: a microstructural analysis, Cem. Concr. Res. (2021), https://doi.org/10.1016/j.cemconres.2020.106303.

[38] L. Bodnárová, J. Válek, L. Sitek, J. Foldyna, Effect of high temperatures on cement composite materials in concrete structures, Acta Geodyn. Geomater. (2013), https://doi.org/10.13168/AGG.2013.0017.

[39] I. Ramón-Álvarez, C. Marugán-Cruz, E. Enríquez, S. Sánchez-Delgado, M. Torres-Carrasco, Alkali-activated and hybrid materials: alternative to Portland cement as a storage media for solar thermal energy, Boletín La Soc. Española Cerámica y Vidr (2021), https://doi.org/10.1016/j.bsecv.2021.11.006.

[40] M. Torres-Carrasco, F. Puertas, Waste glass as a precursor in alkaline activation: chemical process and hydration products, Construct. Build. Mater. 139 (2017) 342–354, https://doi.org/10.1016/j.conbuildmat.2017.02.071.

[41] A. Fernández-Jiménez, I. Garcia-Lodeiro, O. Maltseva, A. Palomo, Hydration mechanisms of hybrid cements as a function of the way of addition of chemicals, J. Am. Ceram. Soc. 102 (2019) 427–436, https://doi.org/10.1111/jace.15939.
[42] I. Peralta, A. Caggiano, I. Ram, S. Sergio, M. Torres-carrasco, Experimental and Computational Optimization of Eco-Friendly Mortar Blocks for High Temperature Thermal Energy Storage of Concentrated Solar Power Plants, vol. 71, 2023, https://doi.org/10.1016/j.est.2023.108076.
[43] M. Torres-Carrasco, E. Enríquez, L. Terrón-menoyo, M.J. Cabrera, D. Muñoz, J.F. Fernández, Improvement of thermal efficiency in cement mortars by using synthetic feldspars, Construct. Build. Mater. (2020) 121279, https://doi.org/10.1016/j.conbuildmat.2020.121279.
[44] E. Enríquez, M. Torres-Carrasco, M.J. Cabrera, D. Muñoz, J.F. Fernández, Towards more sustainable building based on modified Portland cements through partial substitution by engineered feldspars, Construct. Build. Mater. (2020), https://doi.org/10.1016/j.conbuildmat.2020.121334.
[45] L.D. Hung Anh, Z. Pásztory, An overview of factors influencing thermal conductivity of building insulation materials, J. Build. Eng. (2021), https://doi.org/10.1016/j.jobe.2021.102604.
[46] S. Luhar, D. Nicolaides, I. Luhar, Fire resistance behaviour of geopolymer concrete: an overview, Buildings (2021), https://doi.org/10.3390/buildings11030082.
[47] F. Kantarci, İ. Türkmen, E. Ekinci, Improving elevated temperature performance of geopolymer concrete utilizing nano-silica, micro-silica and styrene-butadiene latex, Construct. Build. Mater. (2021), https://doi.org/10.1016/j.conbuildmat.2021.122980.
[48] M.M. Shoaib, S.A. Ahmed, M.M. Balaha, Effect of fire and cooling mode on the properties of slag mortars, Cem. Concr. Res. (2001), https://doi.org/10.1016/S0008-8846(01)00561-0.
[49] D. Laing, C. Bahl, T. Bauer, M. Fiss, N. Breidenbach, M. Hempel, High-temperature solid-media thermal energy storage for solar thermal power plants, in: Proc. IEEE, 2012, https://doi.org/10.1109/JPROC.2011.2154290.
[50] N.K. Lee, K.T. Koh, G.H. An, G.S. Ryu, Influence of binder composition on the gel structure in alkali activated fly ash/slag pastes exposed to elevated temperatures, Ceram. Int. (2017), https://doi.org/10.1016/j.ceramint.2016.11.042.
[51] C.L. Chan, M. Zhang, Behaviour of strain hardening geopolymer composites at elevated temperatures, Cem. Concr. Compos. 132 (2022) 104634, https://doi.org/10.1016/j.cemconcomp.2022.104634.
[52] P. Duan, C. Yan, W. Zhou, W. Luo, C. Shen, An investigation of the microstructure and durability of a fluidized bed fly ash-metakaolin geopolymer after heat and acid exposure, Mater. Des. (2015), https://doi.org/10.1016/j.matdes.2015.03.009.
[53] UNE-EN 196-1, UNE-EN 196-1 Métodos de ensayo de cementos - Parte 1: Determinación de resistencias mecánicas, Eur. Stand, 2005.
[54] A. Fernández-Jiménez, I. Garcia-Lodeiro, O. Maltseva, A. Palomo, Hydration mechanisms of hybrid cements as a function of the way of addition of chemicals, J. Am. Ceram. Soc. (2019), https://doi.org/10.1111/jace.15939.
[55] S. Shagñay, L. Ramón, M. Fernández-álvarez, A. Bautista, F. Velasco, M. Torres-Carrasco, Eco-efficient hybrid cements: pozzolanic, mechanical and abrasion properties, Appl. Sci. 10 (2020) 1–15, https://doi.org/10.3390/app10248986.
[56] AENOR, UNE-EN 196-3:2017. Métodos de ensayo de cementos. Parte 3: Determinación del tiempo de fraguado y de la estabilidad de volumen, 2017, pp. 3–6.
[57] R. Fowler, E.A. Guggenheim, Staatistical thermodynamics: a version of statistical mechanics for students of physics and chemistry, in: Staatistical Thermodyn. A Version Stat, Mech. Students Phys. Chem., 1956.
[58] L. Boquera, J.R. Castro, A.L. Pisello, C. Fabiani, A. D'Alessandro, F. Ubertini, L.F. Cabeza, Thermal and mechanical performance of cement paste under high temperature thermal cycles, Sol. Energy Mater. Sol. Cells (2021), https://doi.org/10.1016/j.solmat.2021.111333.
[59] M. Roig-Flores, T. Lucio-Martin, M.C. Alonso, L. Guerreiro, Evolution of thermo-mechanical properties of concrete with calcium aluminate cement and special aggregates for energy storage, Cem. Concr. Res. (2021), https://doi.org/10.1016/j.cemconres.2020.106323.
[60] T. Lucio-Martin, M. Roig-Flores, M. Izquierdo, M.C. Alonso, Corrigendum to "Thermal conductivity of concrete at high temperatures for thermal energy storage applications: experimental analysis", Sol. Energy 214 (2021) 430–442 https://doi.org/10.1016/j.solener.2021.02.044, 2021.
[61] H. Fu, R. Mo, P. Wang, Y. Wang, Y. Cao, W. Guang, Y. Ding, Influence of elevated temperatures and cooling method on the microstructure development and phase evolution of alkali-activated slag, Materials (2022), https://doi.org/10.3390/ma15062022.
[62] R.P. Selvam, M. Castro, 3D FEM model to improve the heat transfer in concrete for thermal energy storage in solar power generation, in: ASME 2010 4th Int. Conf. Energy Sustain. ES, 2010, 2010, https://doi.org/10.1115/ES2010-90078.
[63] D. Laing, W.D. Steinmann, M. Fiß, R. Tamme, T. Brand, C. Bahl, Solid media thermal storage development and analysis of modular storage operation concepts for parabolic trough power plants, J. Sol. Energy Eng. Trans. ASME (2008), https://doi.org/10.1115/1.2804625.